Collider signatures of dark *CP* violation

A. Cordero-Cid,[1,*] J. Hernández-Sánchez,[1,†] V. Keus,[2,3,‡] S. Moretti,[3,4,§] D. Rojas-Ciofalo,[3,‖] and D. Sokołowska[5,¶]

[1]*Instituto de Física and Facultad de Ciencias de la Electrónica, Benemérita Universidad Autónoma de Puebla, Apdo. Postal 542, C.P. 72570 Puebla, México*

[2]*Department of Physics and Helsinki Institute of Physics, Gustaf Hallstromin katu 2, University of Helsinki, 00014 Helsinki, Finland*

[3]*School of Physics and Astronomy, University of Southampton, Southampton SO17 1BJ, United Kingdom*

[4]*Particle Physics Department, Rutherford Appleton Laboratory, Chilton, Didcot, Oxon OX11 0QX, United Kingdom*

[5]*International Institute of Physics, Universidade Federal do Rio Grande do Norte, Campus Universitario, Lagoa Nova, Natal-RN 59078-970, Brazil*

(Received 19 February 2020; accepted 27 April 2020; published 18 May 2020)

We study an extension of the Standard Model (SM) in which two copies of the SM-Higgs doublet which do not acquire a vacuum expectation value, and hence are *inert*, are added to the scalar sector. The lightest particle from the inert sector, which is protected from decaying to SM particles through the conservation of a Z_2 symmetry, is a viable dark matter candidate. We allow for *CP* violation in this extended dark sector and evaluate the ZZZ vertex and its *CP*-violating form factor in several benchmark scenarios. We provide collider signatures of this dark *CP* violation in the form of potentially observable asymmetries and cross sections for the $f\bar{f} \to Z^* \to ZZ$ process at both leptonic and hadronic machines.

DOI: 10.1103/PhysRevD.101.095023

I. INTRODUCTION

Since the discovery of what looks like the Standard Model (SM) Higgs boson by the ATLAS and CMS experiments at the CERN Large Hadron Collider (LHC) [1,2] a great effort has been put into establishing detailed properties of this particle. Although, as of now, all measurements are consistent with the SM predictions, it is possible that this discovered scalar is a part of the larger scalar sector.

There is a number of reasons to believe that the SM of particle physics is not complete. Cosmological observations imply that only around 4% of the energy budget of the Universe is explained by baryons [3]. In fact, 85% of matter in the Universe is often assumed to be in the form of nonbaryonic cold, neutral, and weakly interacting dark matter (DM) [4–6], with masses of different proposed candidates varying from a few GeV to a few TeV.

Models with extended scalar sector with a discrete symmetry can provide such a particle, e.g., the inert doublet model (IDM), a 2-Higgs doublet model (2HDM) with an unbroken discrete Z_2 symmetry [7]. The scalar sector of the IDM contains 1 *inert* doublet, which is Z_2-odd, does not develop a vacuum expectation value (VEV) and does not couple to fermions, and 1 *active* Z_2-even Higgs doublet, which has a nonzero VEV and couples to fermions in the same way as the SM Higgs doublet, hence also referred to as I$(1+1)$HDM. The IDM, however constrained, is a viable model that can provide a viable DM candidate (see the latest analyses, e.g., in [8–11]). However, due to the imposed exact Z_2 symmetry, all parameters in the potential are real and there is no room for additional sources of *CP* violation. In order to have *CP* violation and DM in multi-inert doublet models at least three scalar doublets are needed.

In this work we focus on the I$(2+1)$HDM: a 3HDM with 2 inert doublets and 1 active Higgs doublet, where *CP* violation appears purely in the inert sector [12–17]. The other possibility, i.e., I$(1+2)$HDM: a 3HDM with 1 inert doublet plus 2 active Higgs doublets has *CP* violation in the extended active sector [18,19]. However, this leads to significant restrictions on the amount of *CP* violation by SM Higgs data, as the Higgs particle observed at the LHC is very SM-like, and by contributions to the electric dipole moments (EDMs) of electron and neutron [20,21].

*adriana.cordero@correo.buap.mx
†jaime.hernandez@correo.buap.mx
‡Venus.Keus@helsinki.fi
§S.Moretti@soton.ac.uk
‖D.Rojas-Ciofalo@soton.ac.uk
¶dsokolowska@iip.ufrn.br

Published by the American Physical Society under the terms of the Creative Commons Attribution 4.0 International license. Further distribution of this work must maintain attribution to the author(s) and the published article's title, journal citation, and DOI. Funded by SCOAP³.

In the I$(2+1)$HDM the active sector is by construction SM-like.[1] The inert sector contains 6 new scalars, 4 neutral and 2 charged ones. With the introduction of CP violation in the inert sector, the neutral inert particles will have mixed CP quantum numbers. Note that the inert sector is protected by a conserved Z_2 symmetry from coupling to the SM particles, therefore, the amount of CP violation introduced here is not constrained by EDM data. The DM candidate, in this scenario, is the lightest state among the CP-mixed inert states which enlivens yet another region of viable DM mass range, with respect to both I$(1+1)$HDM and CP-conserving I$(2+1)$HDM [12–17].

The layout of the remainder of this paper is as follows. In Sec. II, we present the details of the scalar potential and the theoretical and experimental limits on its parameters as well as our benchmark points (BPs). We then follow with the implementation and calculations of the $f\bar{f} \to Z^* \to ZZ$ process in Sec. III, where f is a generic fermion. In Sec. IV, we discuss observable asymmetries in lepton and hadron colliders. Finally, in Sec. V, we conclude and present the outlook for our future studies.

II. THE I$(2+1)$HDM FRAMEWORK

A. The scalar potential

As discussed in [17], the scalar sector of the model is composed of three scalar doublets:

$$\phi_1 = \begin{pmatrix} H_1^+ \\ \frac{H_1+iA_1}{\sqrt{2}} \end{pmatrix}, \quad \phi_2 = \begin{pmatrix} H_2^+ \\ \frac{H_2+iA_2}{\sqrt{2}} \end{pmatrix}, \quad \phi_3 = \begin{pmatrix} G^+ \\ \frac{v+h+iG^0}{\sqrt{2}} \end{pmatrix}. \tag{1}$$

We impose a Z_2 symmetry on the model under which the fields transform as

$$\phi_1 \to -\phi_1, \quad \phi_2 \to -\phi_2, \quad \phi_3 \to \phi_3, \quad \text{SM} \to \text{SM}. \tag{2}$$

To keep this symmetry exact, i.e., respected by the vacuum, ϕ_1 and ϕ_2 have to be the *inert* doublets, $\langle\phi_1\rangle = \langle\phi_2\rangle = 0$, while ϕ_3 is the *active* doublet, $\langle\phi_3\rangle = v/\sqrt{2} \neq 0$, and plays the role of the SM Higgs doublet. Here, h stands for the SM-like Higgs boson and $G^\pm$, G^0 are the would-be Goldstone bosons.

The resulting Z_2-symmetric potential has the following form [14,22][2]:

$$\begin{aligned} V_{\text{3HDM}} &= V_0 + V_{Z_2}, \\ V_0 &= -\mu_1^2(\phi_1^\dagger\phi_1) - \mu_2^2(\phi_2^\dagger\phi_2) - \mu_3^2(\phi_3^\dagger\phi_3) + \lambda_{11}(\phi_1^\dagger\phi_1)^2 + \lambda_{22}(\phi_2^\dagger\phi_2)^2 + \lambda_{33}(\phi_3^\dagger\phi_3)^2 \\ &\quad + \lambda_{12}(\phi_1^\dagger\phi_1)(\phi_2^\dagger\phi_2) + \lambda_{23}(\phi_2^\dagger\phi_2)(\phi_3^\dagger\phi_3) + \lambda_{31}(\phi_3^\dagger\phi_3)(\phi_1^\dagger\phi_1) \\ &\quad + \lambda'_{12}(\phi_1^\dagger\phi_2)(\phi_2^\dagger\phi_1) + \lambda'_{23}(\phi_2^\dagger\phi_3)(\phi_3^\dagger\phi_2) + \lambda'_{31}(\phi_3^\dagger\phi_1)(\phi_1^\dagger\phi_3), \\ V_{Z_2} &= -\mu_{12}^2(\phi_1^\dagger\phi_2) + \lambda_1(\phi_1^\dagger\phi_2)^2 + \lambda_2(\phi_2^\dagger\phi_3)^2 + \lambda_3(\phi_3^\dagger\phi_1)^2 + \text{H.c.} \end{aligned} \tag{3}$$

All parameters of V_0 are real by construction. The parameters of V_{Z_2} can be complex and therefore it is possible to introduce explicit CP violation in the model. For the relevant[3] complex parameters, we have

$$\lambda_2 = |\lambda_2|e^{i\theta_2}, \qquad \lambda_3 = |\lambda_3|e^{i\theta_3}, \tag{4}$$

with explicit CP-violating phases θ_2 and θ_3. As motivated and discussed in detail in [17], we study the *dark hierarchy* limit where the following relations are imposed:

$$\begin{aligned} &\mu_1^2 = n\mu_2^2, \qquad \text{Re}\lambda_3 = n\text{Re}\lambda_2, \qquad \text{Im}\lambda_3 = n\text{Im}\lambda_2, \\ &\lambda_{31} = n\lambda_{23}, \qquad \lambda'_{31} = n\lambda'_{23}. \end{aligned} \tag{5}$$

In the dark hierarchy limit, the only two relevant complex parameters, λ_2 and λ_3, are related through the relations $|\lambda_3| = n|\lambda_2|$ and $\theta_3 = \theta_2$. The angle θ_2 is therefore the only relevant CP-violating phase and is referred to as θ_{CPV} throughout the paper.

B. Physical scalar states

In the Z_2-conserving minimum of the potential, i.e., at the point $(0, 0, \frac{v}{\sqrt{2}})$ with $v^2 = \frac{\mu_3^2}{\lambda_{33}}$, the resulting mass spectrum of the scalar particles is as follows (as detailed in [17]).

(1) Z_2-even fields from the active doublet, h the SM-like Higgs boson and G^0, $G^\pm$ the Goldstone fields.
(2) Z_2-odd charged inert fields, $S_1^\pm$ and $S_2^\pm$, from the inert doublets.
(3) Z_2-odd CP-mixed neutral inert fields, S_1, S_2, S_3, S_4.

We adopt a notation where $m_{S_1} < m_{S_2} < m_{S_3} < m_{S_4}$, hence choosing S_1 as DM candidate. In the remainder

[1]Tree-level interactions are identical to those of the SM Higgs, with the exception of possible Higgs decays to new states provided they are sufficiently light. At loop level, additional scalar states contribute to Higgs interactions, such as in the $h \to gg, \gamma\gamma$ and $Z\gamma$.

[2]We ignore additional Z_2-symmetric terms that can be added to the potential, e.g., $(\phi_3^\dagger\phi_1)(\phi_2^\dagger\phi_3)$, $(\phi_1^\dagger\phi_2)(\phi_3^\dagger\phi_3)$, $(\phi_1^\dagger\phi_2)(\phi_1^\dagger\phi_1)$ and $(\phi_1^\dagger\phi_2)(\phi_2^\dagger\phi_2)$. as they do not change the phenomenology of the model [17].

[3]The parameter λ_1 can also take a complex value, however, since it is only relevant for dark particle self-interactions, it does not appear in the discussion above. Also, the parameter μ_{12}^2 has a nonphysical phase which can be rotated away.

of the paper, the notations S_1 and DM will be used interchangeably.

C. Constraints on the I(2+1)HDM parameters

The latest theoretical and experimental constrains that are applicable to our studies and the discussion of prospects of detection of the model at future collider experiments are described in details in [17] to which we refer the reader. All considered BPs agree with these constraints.

D. Selection of BPs

Based on the analysis done in our previous papers [12,13,15,16], we have chosen a number of BPs to represent different regions of parameter space in the model. As the aim of the paper is to test the model at colliders, we are focusing here on relatively light masses of DM particles, with $m_{S_1} \lesssim 80$ GeV. In this mass region, the I(2 + 1)HDM provides three distinctive types of benchmark scenarios, as follows.

(1) Scenario A: with a large mass splittings, of order 50 GeV or so, between the DM candidate S_1 and all other inert particles, $m_{S_1} \ll m_{S_2}$, m_{S_3}, m_{S_4}, $m_{S_1^\pm}$, $m_{S_2^\pm}$. Scenarios of this type can be realized within the mass range 53 GeV $\leq m_{\rm DM} \leq$ 75 GeV in agreement with all theoretical and experimental constraints, provided the Higgs-DM coupling, $g_{h\rm DM}$, is relatively small.

(2) Scenario B: with a small mass splitting, of order 20% of $m_{\rm DM}$, between the DM and the next-to-lightest inert neutral particle, $m_{S_1} \sim m_{S_2} \ll m_{S_3}$, m_{S_4}, $m_{S_1^\pm}$, $m_{S_2^\pm}$. This choice also leads to a relatively small mass splitting between S_3 and S_4, effectively separating the neutral sector into two groups, with each generation accompanied by a charged scalar.

(3) Scenario C: with all neutral particles close in mass, $m_{S_1} \sim m_{S_2} \sim m_{S_3} \sim m_{S_4} \ll m_{S_1^\pm} \sim m_{S_2^\pm}$. Across the whole low and medium mass range, this scenario under-produces DM, due to the small mass splittings of the neutral inert particles which in turn strengthen the coannihilation channels, reducing the DM relic density.

(4) Scenario D: which is essentially a scenario A with large ZS_iS_j couplings of order 0.1, and therefore a smaller relic density.

For each BP, we list the input parameters, i.e., masses of particles and all relevant couplings, following the convention:

$$\mathcal{L}_{\rm gauge} \supset g_{ZS_iS_j} Z_\mu (S_i \partial^\mu S_j - S_j \partial^\mu S_i), \tag{6}$$

$$\mathcal{L}_{\rm scalar} \supset \frac{v}{2} g_{S_iS_ih} h S_i^2 + v g_{S_iS_jh} h S_i S_j + v g_{S_i^\pm S_j^\mp h} h S_i^\pm S_j^\mp. \tag{7}$$

TABLE I. The input and derived parameters of our BPs. The masses are given in GeV.

	Point-A	Point-B	Point-C	Point-D
n	0.6	0.5	0.8	0.6
λ'_{23}	−0.16	−0.145	−0.295	−0.169
λ_{23}	0.29	0.171	0.294	0.26
λ_2	0.067	0.013	0.0009	−0.2
$\theta_{\rm CPV}$	$15\pi/16$	$7\pi/8$	$31\pi/32$	$8\pi/15$
μ_2^2	−13800	−15900	−3400	−25300
μ_{12}^2	5050	7950	250	13700
m_{S_1}	72.3	55.4	50.9	63.2
m_{S_2}	103.3	63.2	51.7	78.0
$m_{S_1^\pm}$	106.2	79.1	99.1	106.3
m_{S_3}	129.4	144.3	58.5	185.0
m_{S_4}	155.1	148.8	59.4	213.1
$m_{S_2^\pm}$	157.5	159.2	111.1	204.3
$g_{ZS_1S_2} = g_{ZS_3S_4}$	0.366	0.37	0.37	0.312
$g_{ZS_1S_3} = g_{ZS_2S_4}$	0.0397	0.007	0.0025	0.185
$g_{ZS_1S_4} = g_{ZS_2S_3}$	0.0401	0.007	0.0028	0.07

Table I shows the input and derived parameters for each of the BPs.

III. THE EFFECTIVE *ZZZ* VERTEX

A. The Lorentz structure and the f_4^Z contribution

The *CP*-violating weak basis invariants [23–28], in particular the invariant which represents *CP* violation in the mass matrix, contribute to the effective *ZZZ* vertex. This particular invariant is proportional to the mass splitting between the scalars which mediate the *ZZZ* loop, shown in Fig. 1, the scalar-scalar-*Z* couplings and inversely proportional to the scalar masses [23],

$$J_{CP} \propto \frac{|m_{S_i}^2 - m_{S_j}^2||m_{S_j}^2 - m_{S_k}^2||m_{S_k}^2 - m_{S_i}^2|}{m_{S_i}^2 m_{S_j}^2 m_{S_k}^2} \times |g_{ZS_iS_j}||g_{ZS_jS_k}||g_{ZS_kS_i}|, \tag{8}$$

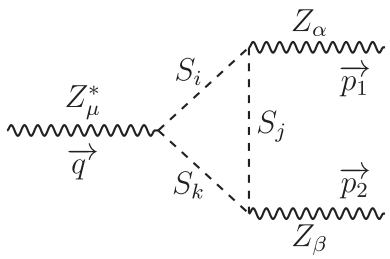

FIG. 1. The one-loop triangle diagram contributing to the f_4^Z factor in the *ZZZ* vertex, mediated by nonidentical scalars S_i, S_j, S_k.

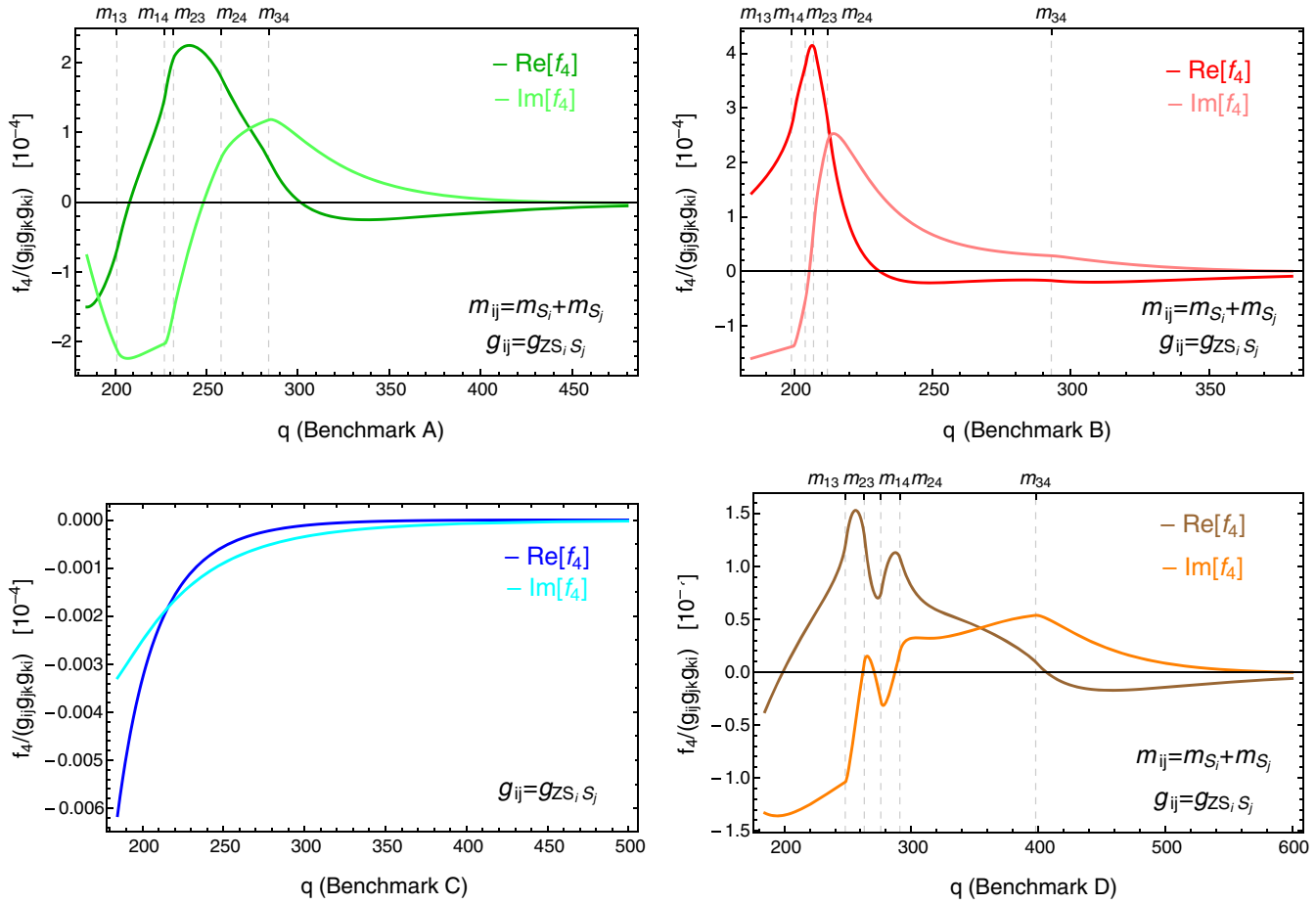

FIG. 2. The f_4^Z value (rescaled by the product of the three ZS_iS_j couplings) in each BP, with respect to the momentum of the off-shell incoming Z^* boson.

where $i \neq j \neq k$, i.e., the scalars in the loop are nonidentical.

In the context of the 2HDM, the CP-violating form factors for triple gauge boson couplings are known [29–31] and have been studied phenomenologically [32–36]. Following the convention of [32,36], the Lorentz structure of the ZZZ vertex when the incoming Z^* boson, characterized by momenta and Lorentz index (q, μ), is assumed to be off-shell and the outgoing Z bosons, characterized by (p_1, α) and (p_2, β), are assumed to be on-shell, as shown in Fig. 1, is reduced to

$$e\Gamma^{\alpha\beta\mu}_{ZZZ} = ie\frac{q^2 - m_Z^2}{m_Z^2}[f_4^Z(q^\alpha g^{\mu\beta} + q^\beta g^{\mu\alpha}) + f_5^Z \epsilon^{\mu\alpha\beta\rho}(p_1 - p_2)_\rho], \tag{9}$$

where e is the proton charge. Also, it is assumed that Z^* couples to a pair of light fermions $f\bar{f}$, hence, the terms proportional to the fermion mass have been neglected. The dimensionless form factor f_4^Z violates CP while f_5^Z conserves CP. In our setup, the f_5^Z contributions are purely from the SM, while the scalar CP violation contributes to f_4^Z solely through the triangle diagram shown in Fig. 1 with $S_iS_jS_k$ in the loop, since the odd Z_2 charge of the inert sector forbids any other diagrams.[4]

Using the package LoopTools [37], we calculate the total one-loop contribution to the f_4^Z factor in our model to be given by a linear combination of the three-point tensor coefficient functions C_{002} (in the LoopTools notation) as:

$$f_4^Z = \frac{m_Z^2}{2\pi^2 e(q^2 - m_Z^2)}|g_{ZS_2S_3}||g_{ZS_1S_3}||g_{ZS_1S_2}| \times \sum_{i,j,k}^{4} \epsilon_{ijk} C_{002}(m_Z^2, m_Z^2, q^2, m_i^2, m_j^2, m_k^2), \tag{10}$$

where $m_{i,j,k}$ stands for the mass of the $S_{i,j,k}$ scalar. Figure 2 shows the value of f_4^Z (rescaled by the product of the three ZS_iS_j couplings) with respect to the momentum of the off-shell incoming Z^* boson, q, for all our BPs. Here, for cases A, B, and D, we have highlighted the mass thresholds

[4]For example, triangle diagrams where one neutral inert scalar is replaced by a neutral Goldstone G_0 or a Z boson.

inside the loop at $q = m_{ij} = m_{S_i} + m_{S_j}$. The mass thresholds in point C appear around 100 GeV which is well below the energy required for a ZZ final state. As expected from Eq. (8), BPs with larger scalar mass splittings have a larger f_4^Z contribution, namely points A, B, and D, while small mass splittings lead to a small f_4^Z contribution, as in point C.

B. The $f\bar{f} \to Z^* \to ZZ$ cross section

The expression in Eq. (9) can be extracted from the following effective Lagrangian describing the V^*ZZ coupling ($V = \gamma$, Z) [38–40]:

$$\mathcal{L}_{ZZZ^*} = -\frac{e}{m_Z^2} f_4^Z (\partial_\mu Z^{\mu\beta}) Z_\alpha (\partial^\alpha Z_\beta), \tag{11}$$

where $Z_{\mu\nu} = \partial_\mu V_\nu - \partial_\nu V_\mu$.

Figure 3 shows the differential cross section at the LHC for the $q\bar{q} \to Z^* \to ZZ$ process, i.e., $d\sigma/dM_{ZZ}$ versus M_{ZZ}, obtained with CalcHEP [41] for BPs A, B, and D. We do not show the cross section plots for BP C, since the corresponding f_4^Z is very small. Here, we have used $\sqrt{s} =$ 14 TeV as collider energy and the CTEQ6L1 parton distribution functions (PDFs) [42] with renormalization/factorization scale set equal to M_{ZZ}. Comparing Figs. 2 and 3, it is evident that the cross section plots represent the pattern of the f_4^Z ones for each benchmark scenario with $|f_4^Z| = \sqrt{\mathrm{Re} f_4^{Z2} + \mathrm{Im} f_4^{Z2}}$.

Note that the $q\bar{q} \to ZZ$ process has a large tree-level contribution from the SM, with, e.g., $\sigma(pp \to ZZ) \approx 10\,\mathrm{pb}$ at $\sqrt{s} = 13\,\mathrm{TeV}$ and $\sigma(e^+e^- \to ZZ) \approx 1\,\mathrm{pb}$ at $\sqrt{s} = 200\,\mathrm{GeV}$), whose interference with the one-loop ZZZ process might be observable. However, this interference term is noted to be zero in [33]. We have verified this result by iteratively applying the Dirac equation on the interference term.

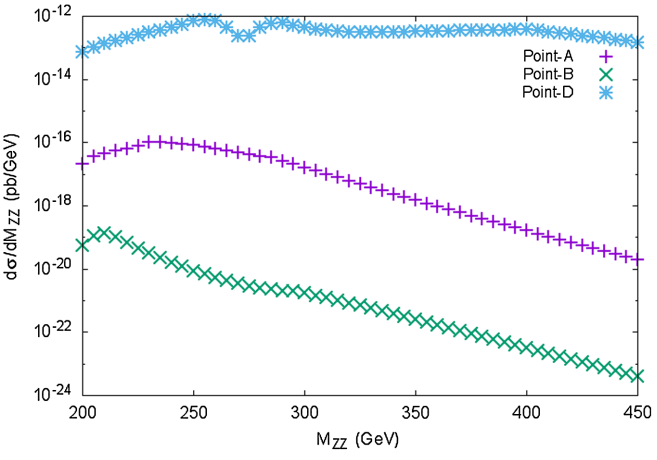

FIG. 3. The differential cross section $d\sigma/dM_{ZZ}$ versus M_{ZZ} for the $q\bar{q} \to Z^* \to ZZ$ process for BPs A, B, and D at the 14 TeV LHC.

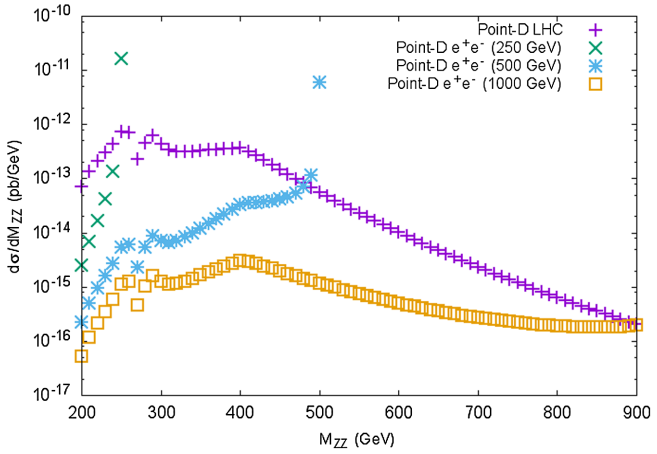

FIG. 4. The differential cross section $d\sigma/dM_{ZZ}$ versus M_{ZZ} for the $f\bar{f} \to Z^* \to ZZ$ process for BP D at the 14 TeV LHC ($f = q$) and a lepton collider ($f = e$) with different energies.

Figure 4 compares the obtained $f\bar{f} \to Z^* \to ZZ$ cross section at the LHC (where $f = q$) and at a lepton collider (where $f = e$). While the result for the hadron collider was obtained considering an energy of 14 TeV, for the lepton collider we considered the energies of 250, 500, and 1000 GeV, which are the values proposed for future e^+e^- colliders such as the Future Circular Collider in e^+e^- mode (FCC-ee), International Linear Collider (ILC), Compact Linear Collider (CLiC) or Circular Electron-Positron Collider (CEPC), see [43] for a comparison of their physics potential. The selected electron/positron PDFs in CalcHEP are the default ones (and we do not include beamsstrahlung effects). Herein, it is remarkable to notice that the LHC distribution generally has a much larger cross section than those at leptonic colliders, except for $M_{ZZ} \approx \sqrt{s}_{e^+e^-}$ (which is natural, as without electron/positron PDFs the distribution would be a δ-function at the lepton collider energy[5]). However, very large luminosities would be required to observe any event at any of these colliders. This is nonetheless a rather novel result, as previous literature exclusively concentrated on e^+e^- colliders, thus overlooking the fact that the LHC generally has more sensitivity to the *CP*-violating contributions entering the ZZZ vertex. Finally, here, we have illustrated this phenomenology for the case of BP D which has the largest cross section among the studied BPs due to its large $g_{ZS_iS_j}$ couplings, but the same pattern is also seen for the other cases.

IV. *CP*-VIOLATING ASYMMETRIES

In an $f\bar{f} \to ZZ$ process, the helicities/polarizations of the ZZ pair can be measured statistically from the angular

[5]A similar effect does not occur at the LHC, where the incoming (anti)quark pair is confined inside the proton beams.

distributions of their decay products. If the helicities/polarizations of the Z bosons are known, one could define CP-violating observables for the ZZ state to test CP violation at future colliders [30,31,36,44–46].

These CP violating observables are defined as differential asymmetries, assuming that both the momenta and helicities of the ZZ pair can be determined (as explained). Since our goal is to measure the CP-violating form factor f_4^Z, these asymmetries will (to leading order) be proportional to f_4^Z.

One can express the cross section σ of the $f\bar{f} \to ZZ$ process as

$$\sigma(f_\delta \bar{f}_{\bar{\delta}} \to Z_\eta Z_{\bar{\eta}}) \equiv \sigma_{\eta,\bar{\eta}} = \sum_{\delta,\bar{\delta}} \mathcal{M}^{\delta,\bar{\delta}}_{\eta,\bar{\eta}}[\Theta]\mathcal{M}^{\star\delta,\bar{\delta}}_{\eta,\bar{\eta}}[\Theta], \quad (12)$$

where $\delta, \bar{\delta}$ are the helicities of the incoming $f, \bar{f}$ and $\eta, \bar{\eta}$ are the helicities of the outgoing ZZ pair, respectively [30]. Following from Eq. (9), the helicity amplitude $\mathcal{M}$ is given as

$$\mathcal{M}_{f\bar{f}\to ZZ} = \frac{1}{q^2 - m_Z^2}\Gamma^{\mu\alpha\beta}_{ZZZ}\epsilon^\alpha(p_1)\epsilon^\beta(p_2)j^\mu(q), \quad (13)$$

where $\epsilon^\alpha(p_1)$ and $\epsilon^\beta(p_2)$ are the polarization vectors of the two outgoing on-shell Z bosons with four momenta p_1 and p_2, respectively. The momentum of the off-shell Z^* boson is characterized by $q = p_1 + p_2$ and the fermionic current with which it connects to the Lagrangian is denoted by j^μ. In the limit where the fermions are assumed to be massless, the j^μ current is conserved, $q_\mu j^\mu = 0$.

In a lepton collider, the angle Θ is defined as the angle between, e.g., the incoming e^- beam direction and the Z whose helicity is given by the first index η. In a hadron collider, we make use of the event boost in the laboratory frame to determine the direction of the incoming particle, i.e., as the boost direction identifies with that of the incoming quark, with respect to which the angle Θ is then measured. Hence, the forthcoming asymmetries, normally studied at lepton colliders, can also be exploited at the LHC.

Here, we introduce three observable asymmetries, namely A^{ZZ}, $\tilde{A}^{ZZ}$, and A''^{ZZ}. Since the two Z bosons in the final state are indistinguishable, for the observation of these asymmetries, one studies the forward hemisphere where one defines the A_1 asymmetry. Then, by studying the backward hemisphere, one defines the A_2 asymmetry. If the asymmetries in the two hemispheres are not equal, i.e., $A_1 - A_2 \neq 0$, one can confidently claim that the model is CP violating.

A. Asymmetries A_1^{ZZ} and A_2^{ZZ}

The A_1^{ZZ} and A_2^{ZZ} asymmetries are defined as

$$A_1^{ZZ} \equiv \frac{\sigma_{+,0} - \sigma_{0,-}}{\sigma_{+,0} + \sigma_{0,-}}, \qquad A_2^{ZZ} \equiv \frac{\sigma_{0,+} - \sigma_{-,0}}{\sigma_{0,+} + \sigma_{-,0}}, \quad (14)$$

where $\sigma_{\eta,\bar{\eta}}$, as defined in Eq. (12), is the unpolarized beam cross section for the production of ZZ with helicities η and $\bar{\eta}$. With this definition, A_1^{ZZ} and A_2^{ZZ} are calculated to be

$$A_1^{ZZ} = -4\beta[(1+\beta^2)^2 - (2\beta\cos\Theta)^2]\gamma^4\mathcal{F}_1(\beta,\Theta)\mathrm{Im}f_4^Z,$$
$$A_2^{ZZ} = A_1^{ZZ}(\cos\Theta \to -\cos\Theta), \quad (15)$$

to the lowest order in f_4^Z, where $\gamma = M_{ZZ}/(2m_Z)$ and $\beta^2 = 1 - \gamma^{-2}$. The prefactor $\mathcal{F}_1(\beta,\Theta)$ is defined as

$$\mathcal{F}_1(\beta,\Theta) = \frac{N_0 + N_1\cos\Theta + N_2\cos^2\Theta + N_3\cos^3\Theta}{D_0 + D_1\cos\Theta + D_2\cos^2\Theta + D_3\cos^3\Theta + D_4\cos^4\Theta}, \quad (16)$$

with the following coefficients

$$\xi_1 = \sin\theta_W\cos\theta_W(1 - 6\sin^2\theta_W + 12\sin^4\theta_W),$$
$$\xi_2 = 16\sin^7\theta_W\cos\theta_W,$$
$$\xi_3 = 1 - 8\sin^2\theta_W + 24\sin^4\theta_W - 32\sin^6\theta_W, \quad \xi_4 = 32\sin^8\theta_W,$$
$$N_0 = (1+\beta^2)\xi_1, \quad N_1 = -2\beta^2(\xi_1 - \xi_2),$$
$$N_2 = (\beta^2 - 3)\xi_1, \quad N_3 = 2(\xi_1 - \xi_2),$$
$$D_0 = (1+\beta^2)^2(\xi_3 + \xi_4), \quad D_1 = 2(1-\beta^4)\xi_3,$$
$$D_2 = -(3 + 6\beta^2 - \beta^4)(\xi_3 + \xi_4), \quad D_3 = -4(1-\beta^2)\xi_3,$$
$$D_4 = 4(\xi_3 + \xi_4). \quad (17)$$

For all our BPs, we show these asymmetries in Fig. 5 for three values of invariant mass of the outgoing ZZ pair, M_{ZZ}. Note that $M_{ZZ} \neq \sqrt{s}_{e^+e^-}$ as we include bremsstrahlung photons from the initial state.

B. Asymmetries $\tilde{A}_1^{ZZ}$ and $\tilde{A}_2^{ZZ}$

Other CP-violating observables are the $\tilde{A}_1^{ZZ}$ and $\tilde{A}_2^{ZZ}$ asymmetries, defined as

$$\tilde{A}_1^{ZZ} \equiv \frac{\sigma_{+,0} + \sigma_{0,+} - \sigma_{0,-} - \sigma_{-,0}}{\sigma_{+,0} + \sigma_{0,+} + \sigma_{0,-} + \sigma_{-,0}},$$
$$\tilde{A}_2^{ZZ} \equiv \frac{\sigma_{+,0} - \sigma_{0,+} - \sigma_{0,-} + \sigma_{-,0}}{\sigma_{+,0} + \sigma_{0,+} + \sigma_{0,-} + \sigma_{-,0}}. \quad (18)$$

Calculating these asymmetries to leading order in f_4^Z reduces their expressions to

$$\tilde{A}_1^{ZZ} = \left[\frac{-2\beta[(1+\beta^2)^2 - (2\beta\cos\Theta)^2][1+\beta^2-(3-\beta^2)\cos^2\Theta]}{(1+\beta^2)^2 - (3+6\beta^2-\beta^4)\cos^2\Theta + 4\cos^4\Theta}\right] \times\gamma^4\xi\mathrm{Im}f_4^Z,$$
$$\tilde{A}_2^{ZZ} = \left[\frac{-2\beta\cos\Theta[(1+\beta^2)^2 - (2\beta\cos\Theta)^2](\beta^2 - \cos^2\Theta)}{(1+\beta^2)^2 - (3+6\beta^2-\beta^4)\cos^2\Theta + 4\cos^4\Theta}\right] \times\gamma^4\tilde{\xi}\mathrm{Im}f_4^Z, \quad (19)$$

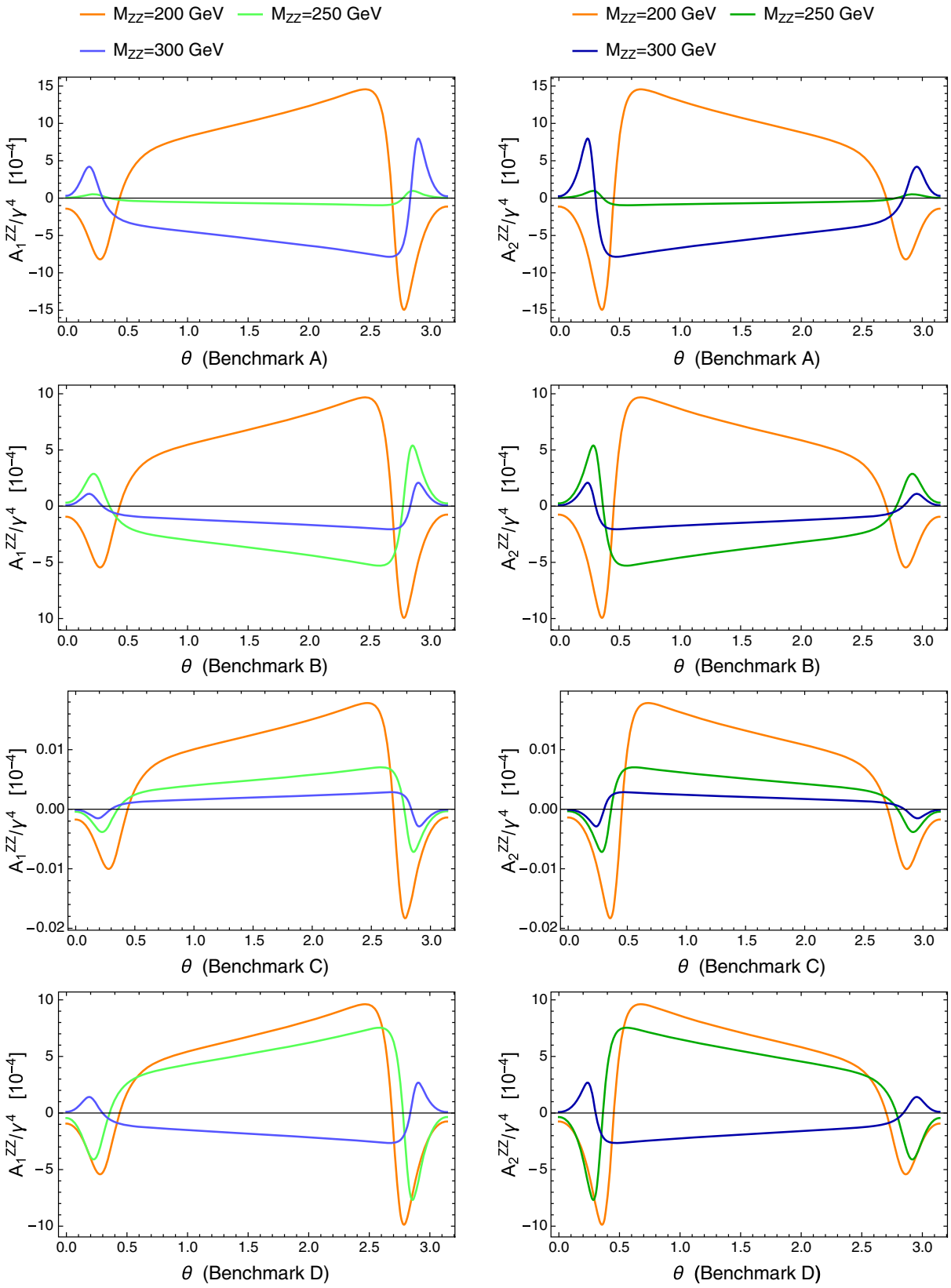

FIG. 5. The asymmetries $A_1^{ZZ}(\Theta)$ and $A_2^{ZZ}(\Theta)$ as functions of Θ for three values of M_{ZZ}, the invariant mass of the outgoing ZZ particles (in GeV).

where we have defined ξ and $\tilde{\xi}$ to be

$$\xi = \frac{2\sin\theta_W\cos\theta_W(1-6\sin^2\theta_W+12\sin^4\theta_W)}{1-8\sin^2\theta_W+24\sin^4\theta_W-32\sin^6\theta_W+32\sin^8\theta_W},$$
$$\tilde{\xi} = \frac{-4\sin\theta_W\cos\theta_W(1-6\sin^2\theta_W+12\sin^4\theta_W-16\sin^6\theta_W)}{1-8\sin^2\theta_W+24\sin^4\theta_W-32\sin^6\theta_W+32\sin^8\theta_W}, \tag{20}$$

and $\gamma = M_{ZZ}/(2m_Z)$ and $\beta^2 = 1-\gamma^{-2}$ as before.

In Figure 6, we present the $\tilde{A}_1^{ZZ}$ and $\tilde{A}_2^{ZZ}$ asymmetries for all our BPs, again, for three values of M_{ZZ}, the invariant mass of the outgoing ZZ pair.

C. Asymmetries $A_1''^{ZZ}$ and $A_2''^{ZZ}$

To study the helicity formalism of the Z boson pair, it is sufficient to focus on the decay of one outgoing Z boson and study its density matrix, without analyzing the complicated event topology of the 4-fermion final state from the decays of the Z boson pairs [30].

The Hermitian spin-density matrix $\rho_{\eta,\bar{\eta}}$ of the Z boson with the scattering angle Θ (the recoiling Z boson is produced at the scattering angle $\pi-\Theta$) defines the angular distribution of f' in the $Z \to f'\bar{f}'$ decay:

$$\rho(\Theta)_{\eta,\bar{\eta}} = \frac{1}{\mathcal{N}(\Theta)}\sum_{\delta,\bar{\delta},\eta'} \mathcal{M}^{\delta,\bar{\delta}}_{\eta,\eta'}(\Theta)\mathcal{M}^{*\delta,\bar{\delta}}_{\bar{\eta},\eta'}(\Theta), \tag{21}$$

where, again, δ, $\bar{\delta}$ are the helicities of the incoming f, $\bar{f}$ beams and $\eta,\bar{\eta}$ are those of the outgoing Z bosons. Here, $\mathcal{N}$ is a normalization factor which ensures $\mathrm{Tr}(\rho)=1$.

Since the $(+,-)$ or $(-,+)$ components of the spin-density matrix ρ receive the largest CP-violating contribution [30], another observable CP-violating asymmetry is defined as

$$A_1'' = -\frac{1}{\pi}[\mathrm{Im}\rho(\Theta)_{+,-}], \quad A_2'' = \frac{1}{\pi}[\mathrm{Im}\rho(\pi-\Theta)_{-,+}]. \tag{22}$$

Calculating this to the lowest order in f_4^Z, with $\gamma = M_{ZZ}/(2m_Z)$ and $\beta^2 = 1-\gamma^{-2}$, one finds:

$$\mathcal{A}''(\Theta) = A_1'' - A_2'' = \left[\frac{\beta(1+\beta^2)[(1+\beta^2)^2-(2\beta\cos\Theta)^2]\sin^2\Theta}{\pi[2+3\beta^2-\beta^6-\beta^2(9-10\beta^2+\beta^4)\cos^2\Theta-4\beta^4\cos^4\Theta]}\right]\gamma^2\xi\mathrm{Re}f_4^Z, \tag{23}$$

which, unlike other asymmetries defined here, is proportional to the real part of f_4^Z.

Figure 7 shows the $\mathcal{A}''(\Theta)$ asymmetry for all our BPs for three values of invariant mass of the outgoing ZZ pair, M_{ZZ}, as previously.

D. Observability prospects

The results in Fig. 2 and Figs. 5–7 in our I(2 + 1)HDM can be compared with those in the IDM of Ref. [36] and the IDM plus inert singlet of Ref. [40]. Owing to the additional inert (or dark) neutral scalar loop content in our setup (and larger scalar-gauge couplings), we do find significantly larger values of f_4^Z than in either of these two constructs, indeed, up to a factor of 3 or so. This in turn reflects into typically larger values of the asymmetries defined in the previous three subsections with respect to the yield of both the models advocated in Ref. [36] and Ref. [40]. Hence, whenever the corresponding constructs will become testable in a collider environment, so will be the case for ours as well. However, these two publications exclusively concentrated on the scope of future e^+e^- colliders in testing CP-violating effects in the inert (or dark) sector, whereas we have shown here that, when a proper treatment of the initial state dynamics is implemented in e^+e^- annihilations, i.e., electron/positron PDFs are introduced herein, just like in hadronic machines for the (anti)proton content, one finds that the 14 TeV LHC can surpass in sensitivity lepton colliders with energies ranging from 250 to 1000 GeV. In fact, while the differential cross section in M_{ZZ} is more peaked in the latter case, the integral of it over its full kinematic range is larger in the former case. Altogether, the I(2 + 1)HDM would afford one, in selected regions of its parameter space, with asymmetries at the permille level over a sustained range in M_{ZZ}, thus nearly an order of magnitude higher than in the IDM with and without an additional inert singlet. In essence, we claim that observability of "dark CP violation" may well occur sooner rather than later, as the (already approved) high luminosity LHC (HL-LHC) can boast a luminosity comparable to that of many (possible) future electron-positron colliders. However, as already remarked in Refs. [36,40], the full data sample at either machine would be needed to establish any significant effects of CP violation emerging from the inert (or dark) sector, given that the one-loop cross section associated to the imaginary part of the $f\bar{f} \to ZZ$ process is orders of magnitude smaller than that stemming from the real part of it, as this includes a SM tree-level contribution. However, this t, u-channel (tree-level) contribution is topologically different from the s-channel (one-loop) one carrying CP-violating effects, so that one may attempt reducing the first one through an appropriate kinematic selection enhancing the second one. Indeed, there would

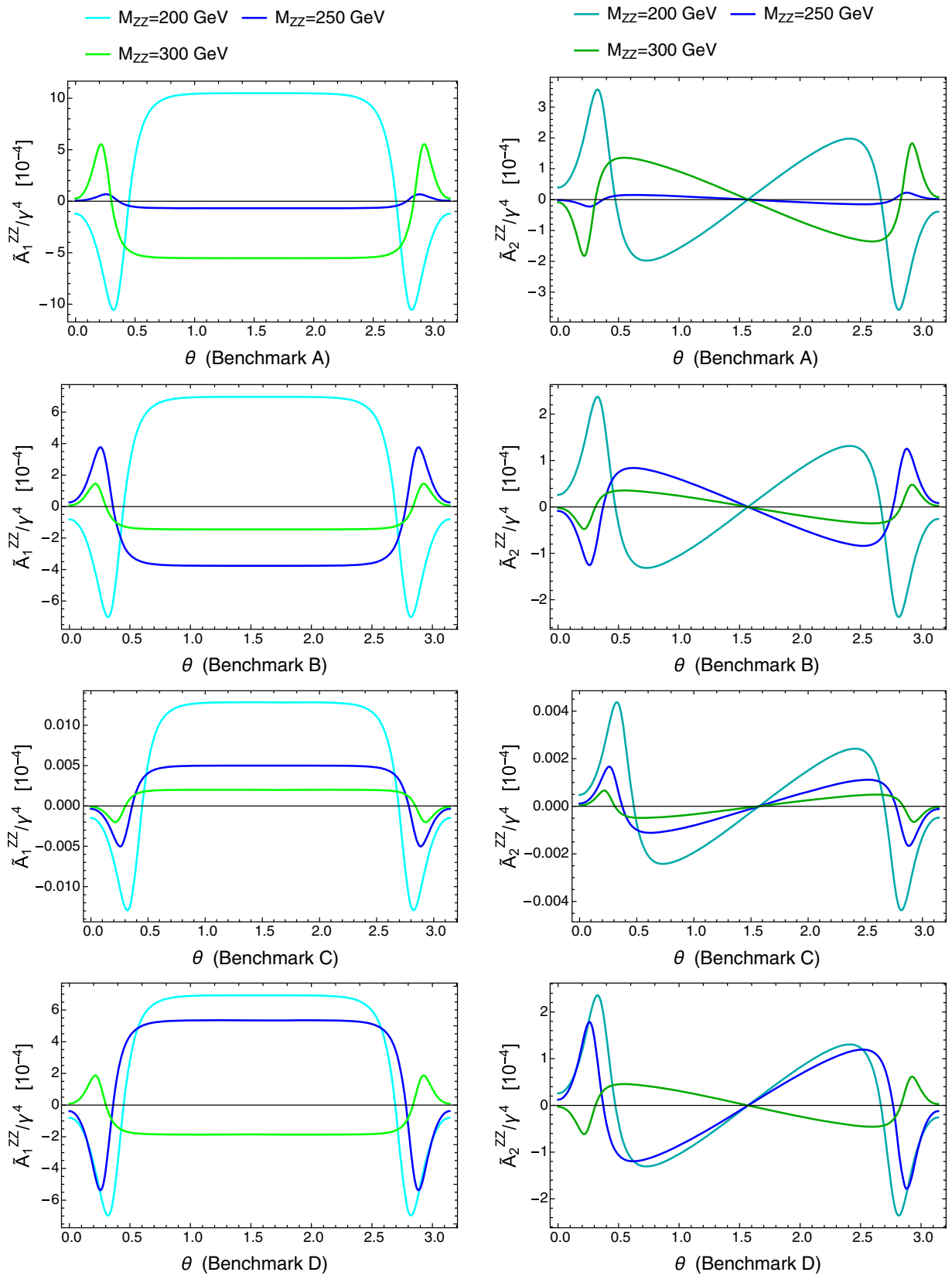

FIG. 6. The asymmetries $\tilde{A}_1^{ZZ}(\Theta)$ and $\tilde{A}_2^{ZZ}(\Theta)$ as functions of Θ for three values of M_{ZZ}, the invariant mass of the outgoing ZZ particles (in GeV).

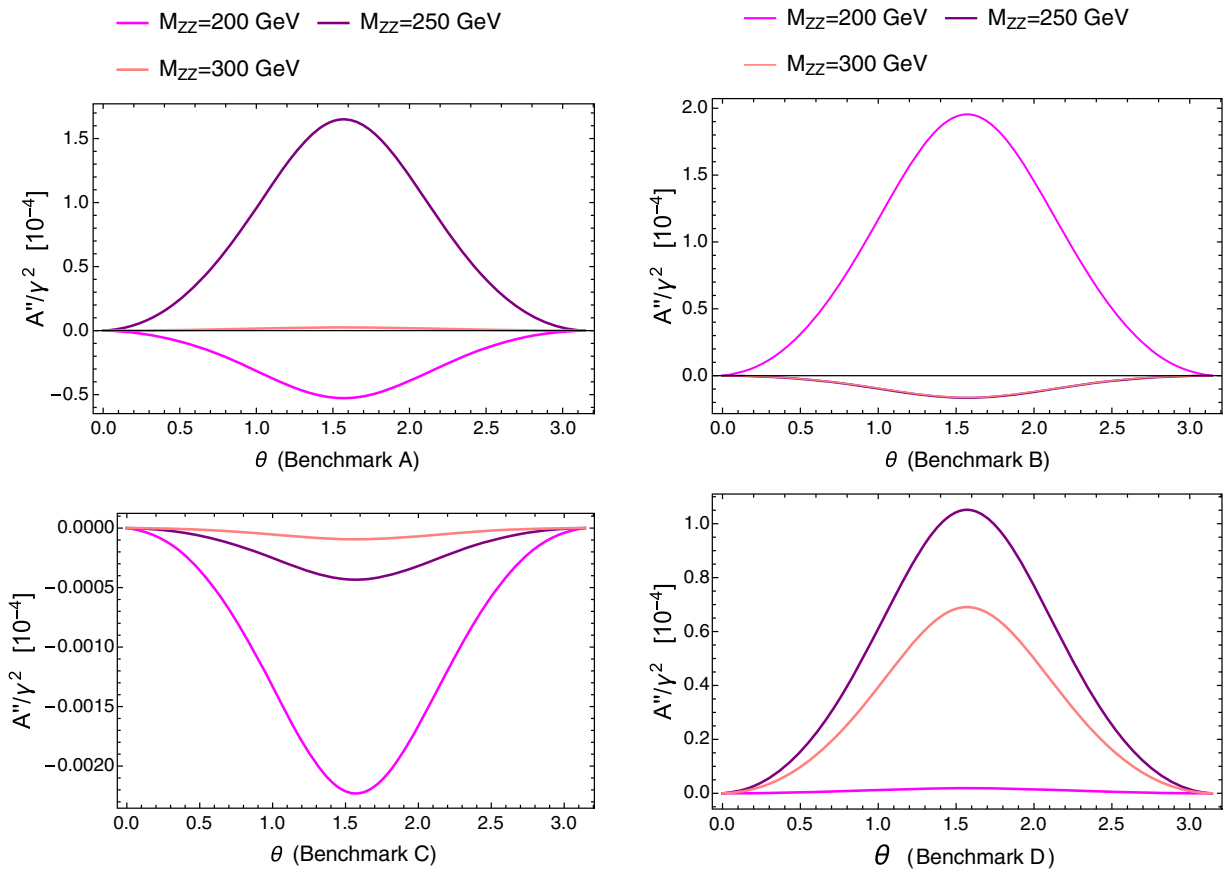

FIG. 7. The asymmetry $\mathcal{A}''(\Theta)$ as a function of Θ for three values of M_{ZZ}, the invariant mass of the outgoing ZZ particles (in GeV).

still remain a topologically irreducible background due to s-channel (one-loop) CP-conserving diagrams (i.e., $f\bar{f} \to Z^* \to ZZ$ via fermionic loops), but this is of the same order as the CP-violating signal, so it should be possible to disentangle these.

V. CONCLUSIONS AND OUTLOOK

In this paper, we have shown that CP violation originating in the inert sector of the I$(2+1)$HDM can make itself manifest in the active one, in fact, in gauge interactions, through one-loop effects entering the cross section for $f\bar{f} \to Z^* \to ZZ$ at the LHC (and future lepton colliders). This process is mediated by neutral Higgs boson triangle topologies triggered by the inert states of the aforementioned framework. Unlike the case of the CP-violating 2HDM, where such effects also exist but are limited in size since one of the three neutral states has to be very SM-like, in the I$(2+1)$HDM all four contributing neutral scalars are inert and can have large gauge couplings. Further, none of the interactions that are generated by the latter can be constrained by EDM data, so that they can all contribute coherently to generate significant asymmetries and increase the cross section for the $f\bar{f} \to Z^* \to ZZ$ process, above and beyond the CP-violating 2HDM yield or that of the 2HDM plus a singlet. The 2HDM plus a singlet case with one active doublet scalar and an inert singlet plus doublet scalars not only has fewer number of inert states contributing to the ZZZ loop, but also has diluted ZS_iS_j couplings since the singlet has no direct couplings to the SM gauge bosons.

In order to illustrate such a phenomenology, we have defined several BPs, each embedding CP violation, over the I$(2+1)$HDM parameter space, with varying mass splittings and coupling strengths in the inert sector, all compliant with available experimental data, from relic density, (in)direct DM searches and colliders. For three such BPs, we have quantified CP violation effects entering three asymmetries which can all be defined in the $q\bar{q} \to Z^* \to ZZ$ channel and potentially measured at both the LHC ($f = q$) by the end of its lifetime (i.e., after the HL-LHC [47,48] runs) and at future lepton colliders ($f = e$) such as the FCC-ee, ILC, CLiC, or CEPC running at current design luminosities. Finally, we have illustrated that the hadronic cross sections are typically larger than the leptonic ones, so that it is quite possible that a first evidence of a CP-violating I$(2+1)$HDM will occur at the LHC rather than at the FCC-ee, ILC, CLiC or CEPC.

ACKNOWLEDGMENTS

S. M. acknowledges support from the Science and Technology Facilities Council (STFC) Consolidated Grant No. ST/L000296/1 and is financed in part through the NExT Institute. S. M., V. K., and D. R.-C. acknowledge the H2020-MSCA-RISE-2014 Grant No. 645722 (NonMinimalHiggs). D. S. is supported in part by the National Science Center, Poland, through the HARMONIA project under Contract No. UMO-2015/18/M/ST2/00518. D.R-C. is supported by the Royal Society Newton International Fellowship NIF/R1/180813. J. H.-S., D. R.-C., and A. C. are supported by CONACYT (México), VIEP-BUAP and PRODEP-SEP (México) under the Grant: "Red Temática: Física del Higgs y del Sabor". V. K. acknowledges financial support from Academy of Finland projects "Particle cosmology and gravitational waves" No. 320123 and "Particle cosmology beyond the Standard Model" No. 310130.

[1] G. Aad *et al.* (ATLAS Collaboration), Phys. Lett. B **716**, 1 (2012).
[2] S. Chatrchyan *et al.* (CMS Collaboration), Phys. Lett. B **716**, 30 (2012).
[3] N. Aghanim *et al.* (Planck Collaboration), arXiv:1807.06209.
[4] G. Jungman, M. Kamionkowski, and K. Griest, Phys. Rep. **267**, 195 (1996).
[5] G. Bertone, D. Hooper, and J. Silk, Phys. Rep. **405**, 279 (2005).
[6] L. Bergstrom, Rep. Prog. Phys. **63**, 793 (2000).
[7] N. G. Deshpande and E. Ma, Phys. Rev. D **18**, 2574 (1978).
[8] A. Ilnicka, M. Krawczyk, and T. Robens, Phys. Rev. D **93**, 055026 (2016).
[9] A. Belyaev, G. Cacciapaglia, I. P. Ivanov, F. Rojas-Abatte, and M. Thomas, Phys. Rev. D **97**, 035011 (2018).
[10] A. Belyaev, S. Moretti, T. R. Fernandez Perez Tomei, S. F. Novaes, P. G. Mercadante, C. S. Moon, L. Panizzi, F. Rojas, and M. Thomas, Phys. Rev. D **99**, 015011 (2019).
[11] J. Kalinowski, W. Kotlarski, T. Robens, D. Sokolowska, and A. F. Zarnecki, J. High Energy Phys. 12 (2018) 081.
[12] V. Keus, S. F. King, S. Moretti, and D. Sokolowska, J. High Energy Phys. 11 (2014) 016.
[13] V. Keus, S. F. King, S. Moretti, and D. Sokolowska, J. High Energy Phys. 11 (2015) 003.
[14] V. Keus, S. F. King, and S. Moretti, J. High Energy Phys. 01 (2014) 052.
[15] A. Cordero-Cid, J. Hernandez-Sanchez, V. Keus, S. F. King, S. Moretti, D. Rojas, and D. Sokolowska, J. High Energy Phys. 12 (2016) 014.
[16] V. Keus, arXiv:1909.09234.
[17] A. Cordero-Cid, J. Hernndez-Snchez, V. Keus, S. Moretti, D. Rojas, and D. Sokoowska, Eur. Phys. J. C **80**, 135 (2020).
[18] B. Grzadkowski, O. M. Ogreid, and P. Osland, Phys. Rev. D **80**, 055013 (2009).
[19] P. Osland, A. Pukhov, G. M. Pruna, and M. Purmohammadi, J. High Energy Phys. 04 (2013) 040.
[20] V. Keus, S. F. King, S. Moretti, and K. Yagyu, J. High Energy Phys. 04 (2016) 048.
[21] V. Keus, N. Koivunen, and K. Tuominen, J. High Energy Phys. 09 (2018) 059.
[22] I. P. Ivanov, V. Keus, and E. Vdovin, J. Phys. A **45**, 215201 (2012).
[23] L. Lavoura and J. P. Silva, Phys. Rev. D **50**, 4619 (1994).
[24] F. J. Botella and J. P. Silva, Phys. Rev. D **51**, 3870 (1995).
[25] J. F. Gunion and H. E. Haber, Phys. Rev. D **72**, 095002 (2005).
[26] B. Grzadkowski, O. M. Ogreid, and P. Osland, J. High Energy Phys. 11 (2014) 084.
[27] H. E. Haber and D. O'Neil, Phys. Rev. D **74**, 015018 (2006); **74**, 059905(E) (2006).
[28] H. E. Haber and O. Stal, Eur. Phys. J. C **75**, 491 (2015); **76**, 312(E) (2016).
[29] X. G. He, J. P. Ma, and B. H. J. McKellar, Phys. Lett. B **304**, 285 (1993).
[30] D. Chang, W. Y. Keung, and P. B. Pal, Phys. Rev. D **51**, 1326 (1995).
[31] D. Chang, W. Y. Keung, and I. Phillips, Phys. Rev. D **48**, 4045 (1993).
[32] K. Hagiwara, R. D. Peccei, D. Zeppenfeld, and K. Hikasa, Nucl. Phys. **B282**, 253 (1987).
[33] G. J. Gounaris, J. Layssac, and F. M. Renard, Phys. Rev. D **61**, 073013 (2000).
[34] G. J. Gounaris, J. Layssac, and F. M. Renard, Phys. Rev. D **65**, 017302 (2001); **62**, 073012(E) (2000).
[35] U. Baur and D. L. Rainwater, Phys. Rev. D **62**, 113011 (2000).
[36] B. Grzadkowski, O. M. Ogreid, and P. Osland, J. High Energy Phys. 05 (2016) 025; 11 (2017) 002(E).
[37] T. Hahn, *Proc. Sci.*, ACAT2010 (2010) 078.
[38] G. J. Gounaris, J. Layssac, and F. M. Renard, Phys. Rev. D **62**, 073013 (2000).
[39] A. Moyotl, J. J. Toscano, and G. Tavares-Velasco, Phys. Rev. D **91**, 093005 (2015).
[40] D. Azevedo, P. M. Ferreira, M. M. Muhlleitner, S. Patel, R. Santos, and J. Wittbrodt, J. High Energy Phys. 11 (2018) 091.

[41] A. Belyaev, N. D. Christensen, and A. Pukhov, Comput. Phys. Commun. **184**, 1729 (2013).
[42] D. Stump, J. Huston, J. Pumplin, W. K. Tung, H. L. Lai, S. Kuhlmann, and J. F. Owens, J. High Energy Phys. 10 (2003) 046.
[43] N. Craig, arXiv:1703.06079.
[44] A. Djouadi *et al.* (ILC Collaboration), arXiv:0709.1893.
[45] P. Lebrun *et al.*, arXiv:1209.2543.
[46] G. Gounaris, D. Schildknecht, and F. M. Renard, Phys. Lett. B **263**, 291 (1991).
[47] F. Gianotti *et al.*, Eur. Phys. J. C **39**, 293 (2005).
[48] A. Abada *et al.* (FCC Collaboration), Eur. Phys. J. Special Topics **228**, 1109 (2019).